

Geophysical Research Letters[®]

RESEARCH LETTER

10.1029/2022GL099123

Key Points:

- Crustal thickness map of northern Borneo obtained from Virtual Deep Seismic Sounding
- Evidence of crustal thinning indicates Sulu Sea extension propagated into northern Borneo during the late Miocene
- Variations in crustal thickness consistent with subduction polarity reversal induced by continent-continent collision

Supporting Information:

Supporting Information may be found in the online version of this article.

Correspondence to:

H. T. Linang,
htal3@cam.ac.uk

Citation:

Linang, H. T., Pilia, S., Rawlinson, N., Bacon, C. A., Gilligan, A., Cornwell, D. G., & Tongkul, F. (2022). Collision-induced subduction polarity reversal explains the crustal structure of northern Borneo: New results from Virtual Deep Seismic Sounding (VDSS). *Geophysical Research Letters*, 49, e2022GL099123. <https://doi.org/10.1029/2022GL099123>








Received 21 JUL 2022

Accepted 30 SEP 2022

© 2022. The Authors.

This is an open access article under the terms of the [Creative Commons Attribution License](#), which permits use, distribution and reproduction in any medium, provided the original work is properly cited.

Collision-Induced Subduction Polarity Reversal Explains the Crustal Structure of Northern Borneo: New Results From Virtual Deep Seismic Sounding (VDSS)

H. T. Linang¹ , S. Pilia^{1,2} , N. Rawlinson¹ , C. A. Bacon¹ , A. Gilligan³ , D. G. Cornwell³ , and F. Tongkul⁴ 

¹Bullard Laboratories, University of Cambridge, Cambridge, UK, ²Department of Earth and Environmental Sciences, University of Milan-Bicocca, Milan, Italy, ³Department of Geology and Geophysics, University of Aberdeen, Aberdeen, UK, ⁴Faculty of Science and Natural Resource, Universiti of Malaysia Sabah, Kota Kinabalu, Malaysia

Abstract Subduction polarity reversal (SPR) is a key subduction initiation mechanism often associated with arc-continent collision zones. Northern Borneo has long been recognized as a location where sequential but opposing subduction zones were present in the Miocene, but has not been examined in the context of SPR. Here, we exploit teleseismic data from northern Borneo to investigate crustal thickness variations using Virtual Deep Seismic Sounding (VDSS). Our results reveal a thick crustal root beneath the Crocker Range and an area of relatively thin crust in the southeast, which appears to extend northeast into the Sulu Sea, where back-arc rifting behind the younger subduction zone developed. Overall, our findings are consistent with predictions from numerical models of SPR involving arc-continent collision, but with several important differences—including a substantial mountain range and more limited back-arc rifting that can be attributed to northern Borneo being an example of SPR involving continent-continent collision.

Plain Language Summary Northern Borneo lies in the heart of Southeast Asia and was assembled by a complex series of tectonic events over the last 40 million years. Principle among these was the subduction of the Proto South China Sea plate beneath its northwest continental margin, which ended in continent-continent collision. Subduction of the Celebes Sea plate in the southwest followed, which terminated ~9 million years ago. In this study, we exploit seismic data collected in northern Borneo to construct a new crustal model of the region, that robustly constrains the crust-mantle boundary. We find that crustal thickness variations are consistent with a subduction polarity reversal (SPR) event induced by continent-continent collision, with thicker crust underlying the collision zone and thinner crust related to extension driven by retreat of the younger subduction zone. Our results have important implications for the study of SPR and subduction initiation and the processes that influence post-subduction tectonic settings.

1. Introduction

In the last decade, subduction initiation (SI) has become firmly established as one of the most exciting and rapidly developing fields of modern plate tectonics thanks to improved observations, more realistic geodynamic modeling and more focused laboratory experiments (Stern & Gerya, 2018). Subduction polarity reversal (SPR), a compression-induced form of SI in which intra-oceanic subduction is followed by collision, subduction termination, slab break-off, initiation of subduction of opposite polarity behind the collision zone, orogen collapse and back-arc spreading driven by roll-back, has become a particular focus of the geodynamic modeling community in the last few years (e.g., Almeida et al., 2022; Stern & Gerya, 2018; Wang et al., 2022; Yang, 2022). Typical models are 2-D and involve arc-continent (Wang et al., 2022) or oceanic plateau-continent collision (Almeida et al., 2022). Type examples of these collision styles that can be used to validate numerical modeling results include the Andaman Arc, Banda Arc, Kamchatka Orogen, and Taiwan Orogen. Useful constraints can also be found in the geological record; for instance, Gasser et al. (2022) study the Laurentian Iapetus margin and find evidence for all key stages of SPR from a detailed petrological analysis of Ordovician outcrop. Although SI is largely thought to be compression-driven, numerical modeling suggests that slab break-off can induce mantle flow, which can cause back-arc lithosphere to rupture and be pulled down into the mantle (Wang et al., 2022).

Northern Borneo, which incorporates the Malaysian state of Sabah, hosts two opposed subduction systems that sequentially terminated in the Miocene (e.g., Hall, 2013; Hall et al., 2008; Hutchinson et al., 2000; Tongkul, 2017).

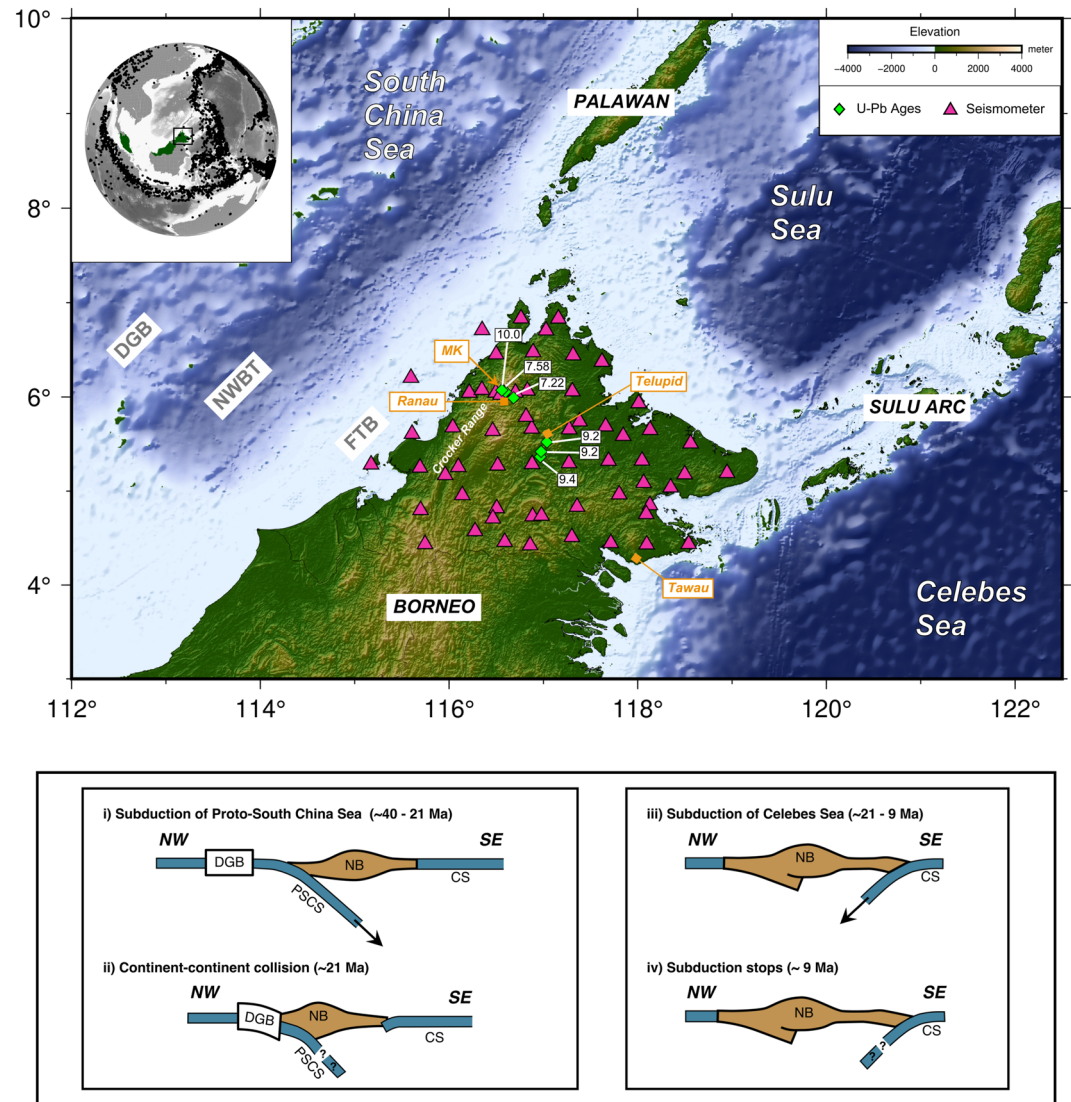


Figure 1. Map of the study area. Magenta triangles show seismic stations from northern Borneo Orography Seismic Survey and MetMalaysia networks. Green diamonds denote geochemical dating locations relevant to this study. Top-left inset shows the SE Asia region with Malaysia in green and Sabah highlighted by a black rectangle. DGB, Dangerous Grounds Block; NWBT, NW Borneo Trough; FTB, Fold and Thrust Belt; MK, Mt. Kinabalu. The bottom panel is a schematic illustration of the tectonic evolution of northern Borneo that is consistent with Hall (2013).

Subduction of the Proto-South China Sea (PSCS) beneath NW northern Borneo began in the Eocene and ceased in the Early Miocene when continent-continent collision between the Dangerous Grounds block (see Figure 1) and the western margin of northern Borneo occurred (Hall & Breiffeld, 2017). Subsequently, NW subduction of the Celebes Sea beneath the Sulu Sea began around 21 Ma and terminated at ~9 Ma (Lai et al., 2021).

Due to its complex geology being masked by tropical vegetation and limited constraints on deep structure, the Neogene evolution of northern Borneo remains controversial, with explanations ranging between predominantly compressional (Morley & Back, 2008; Morley et al., 2011; Tongkul, 1994, 1997) and extensional tectonics (Hall, 2013; Pilia, Davies, et al., 2021). However, no study has yet considered the tectonic evolution of northern Borneo in the context of SPR and the typical sequence of events it entails. With the recent completion of the northern Borneo Orography Seismic Survey (nBOSS) seismic experiment in northern Borneo, new data are now available that can help determine whether this may have occurred.

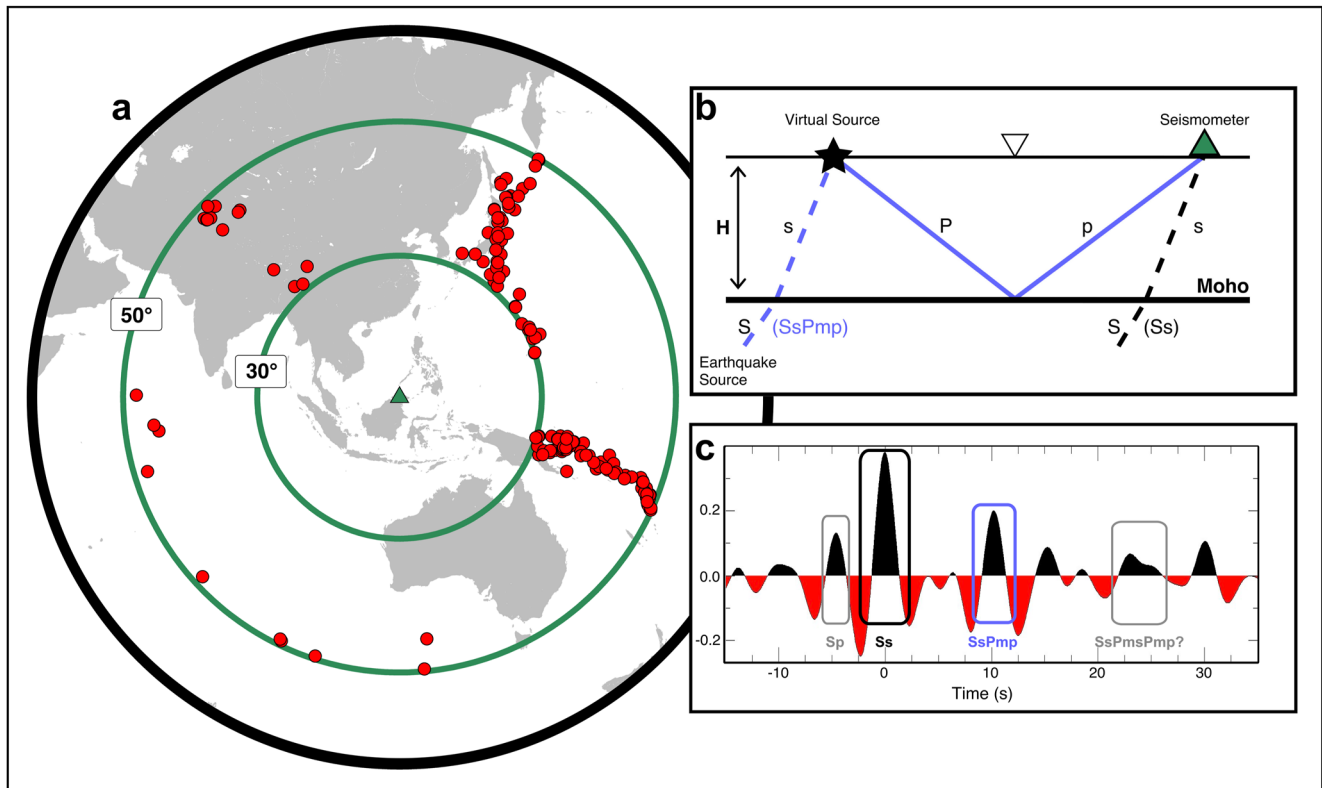


Figure 2. (a) Seismic source distribution (red dots) in the epicentral distance range 30°–50° from which earthquake data were extracted. (b) Schematic ray diagram illustrating the main phases used during the Virtual Deep Seismic Sounding analysis. (c) Stacked waveform data example from a station in northern Borneo with the Ss and SsPmp arrivals highlighted in black and blue, respectively. The precursor Sp phase and reverberatory SsPmsPmp are highlighted in gray.

In this study, we utilize nBOSS teleseismic waveform data to estimate Moho depth variations beneath northern Borneo by exploiting a recently developed passive seismic method called Virtual Deep Seismic Sounding (VDSS), initially proposed by Tseng et al. (2009). We followed and implemented the method as in Thompson et al. (2019) and Pilia, Ali, et al. (2021) to obtain estimates of crustal thickness beneath northern Borneo. Our primary aim in this study is to assess whether crustal thickness variations appear consistent with SPR induced by continent-continent collision, as determined by numerical modeling and other observational studies.

2. Virtual Deep Seismic Sounding

We exploit waveform data recorded by 45 broadband stations of the nBOSS temporary seismic network and 20 broadband stations operated by MetMalaysia (Pilia et al., 2019)—see Figure 1 for locations. In total, 294 earthquakes with magnitudes ≥ 5.0 in a 30°–50° epicentral distance range from the station (Figure 2a) are used. VDSS focuses on the SsPmp phase, originating from an S-to-P conversion at the free surface. The converted P-wave then travels downwards and undergoes a wide-angle (post-critical) reflection at the Moho before impinging on a seismic station (Figure 2b). The difference in arrival time between the SsPmp phase and the Ss phase ($T_{\text{SsPmp-Ss}}$) provides an estimate of the Moho depth through the following equation:

$$T_{\text{SsPmp-Ss}} = 2H (V_p^{-2} - p_\beta^2)^{1/2} \quad (1)$$

where H is the crustal thickness, V_p is the average P-wave speed in the crust, and p_β is the ray parameter, which is determined using the known source-receiver geometry and the ak135 velocity model (Kennett et al., 1995).

The first step in preparing a VDSS trace is to isolate the SsPmp phase from its event waveform. This involves windowing data around the S-arrival time generated by a teleseismic source, using predictions from ak135. The instrument response is then deconvolved from the raw data before applying a second-order zero-phase

Butterworth bandpass filter with 0.05 and 0.5 Hz corner frequencies. The horizontal components are then rotated into radial and tangential components (Thompson et al., 2019). In order to remove source-side scattering effects, we applied the source normalization method of Yu et al. (2013), which allows the use of all seismic events within the prescribed epicentral distance range regardless of focal depth.

Next, the vertical and radial component traces are rotated into pseudo-S component traces (Parker et al., 2016; Thompson et al., 2019), an estimate of the shear wave source wavelet, which is then deconvolved from the vertical and radial component of the waveform using an extended-time multitaper approach (10 s sliding window, 75% window overlap, 3 Slepian tapers; Helffrich, 2006), which helps to isolate the SsPmp impulse response. The resulting vertical component VDSS traces are visually inspected and retained if: (a) the SsPmp phase is clearly visible; (b) a prominent direct Ss arrival and precursor sP can be detected; and (c) ringy or oscillatory signals are absent. Finally, we use the seismic model from a joint receiver function (RF) and surface wave inversion analysis (Pilia, Davies, et al., 2021) to produce synthetic seismograms and get the predicted travel time of the SsPmp phase for different slownesses at each station. Traces are retained if their SsPmp arrival (at the first zero-crossing in our case) falls within 4-seconds before or after the zero-crossing of the synthetic SsPmp phase arrival. S-wave velocities estimated beneath each station (see Figure S1 in Supporting Information S1) obtained from the RF analysis are converted to P-wave velocities using the empirical relation devised by Brocher (2005), which allows us to estimate bulk velocity V_p . Finally, we perform a time-to-depth migration of each VDSS trace based on Equation 1.

In this study, the SsPmp phase is observed across the range between 14.2 and 15.7 s/deg, which delivers a clear post-critical reflection of the P-wave at the Moho, but also a phase shift and moveout (see Figure S2 in Supporting Information S1). Liu et al. (2018) analyzed other potential limitations of the VDSS method, and concluded that the SsPmp arrival time could be affected by several conditions, including (a) variation in the P-wave velocity of the lower crust and upper mantle, (b) lateral heterogeneity in the crust and upper mantle, (c) near-surface velocity at the virtual source, and (d) the presence of a gradational crust-mantle boundary. Liu et al. (2020) performed synthetic tests with 2D models, and found that the SsPmp phase (travel time, phase shift, and amplitude) can also be affected by lateral variations in lithospheric seismic structure. Thompson et al. (2019) also tested several limitations inherent to VDSS and showed that when armed with a relatively large number of sources characterized by a good slowness coverage, stacking of the VDSS waveforms can average out any bias that the phase shift might introduce. Their study also showed that the effect of phase shift can be removed by calculating the envelope function of individual VDSS traces; however, they found that the zero-crossing proxy and envelope function results are consistent when a good slowness coverage is present, as it is in our case.

There are two main approaches for obtaining final crustal thickness results from VDSS. One (method A) is to consider depth-to-Moho estimates from every single trace at the reflection point of the Pmp leg located at the base of the crust (e.g., Matchette-Downes et al., 2019; Tseng et al., 2009; Yu et al., 2016). This approach has the advantage of considering the crustal thickness at the reflection location and is often favored when a small number of seismic sources are used; however, the zero-crossing proxy would overestimate the crustal thickness at low slowness and vice-versa for high slowness. Another way (method B) is to stack all available VDSS traces to produce a final VDSS trace from which crustal thickness beneath a station is estimated from the SsPmp zero-crossing (Pilia, Ali, et al., 2021; Thompson et al., 2019). This has the advantage of mitigating the phase-shift effect, averaging out errors caused by lateral velocity heterogeneity, and boosting the SNR of the SsPmp phase. However, this comes at the expense of lateral resolution since the footprint of the single station measurement extends radially outwards to encompass every Pmp reflection point. We apply both methods A and B to our teleseismic waveform data from northern Borneo, and jointly consider the results.

3. Results

Figures 3b and 3d illustrate the final Moho-depth map of northern Borneo obtained using VDSS methods A and B, respectively, which reveals several alternating thin and thick crustal bands, with depths ranging between 20 and 45 km. The good consistency between our results and those from the receiver functions (Figure 3c), which involves a near-vertical incidence Ps phase and associated reflections and mode conversions, suggests that the effect of lateral heterogeneity in the mantle appears to be minimal in our case. To confirm this, we followed the approach of Yu et al. (2016). For each source-receiver pair, we calculated the relative S-wave arrival time residual of the direct Ss phase before extracting the Ss leg of the SsPmp phase at the virtual source location. The difference

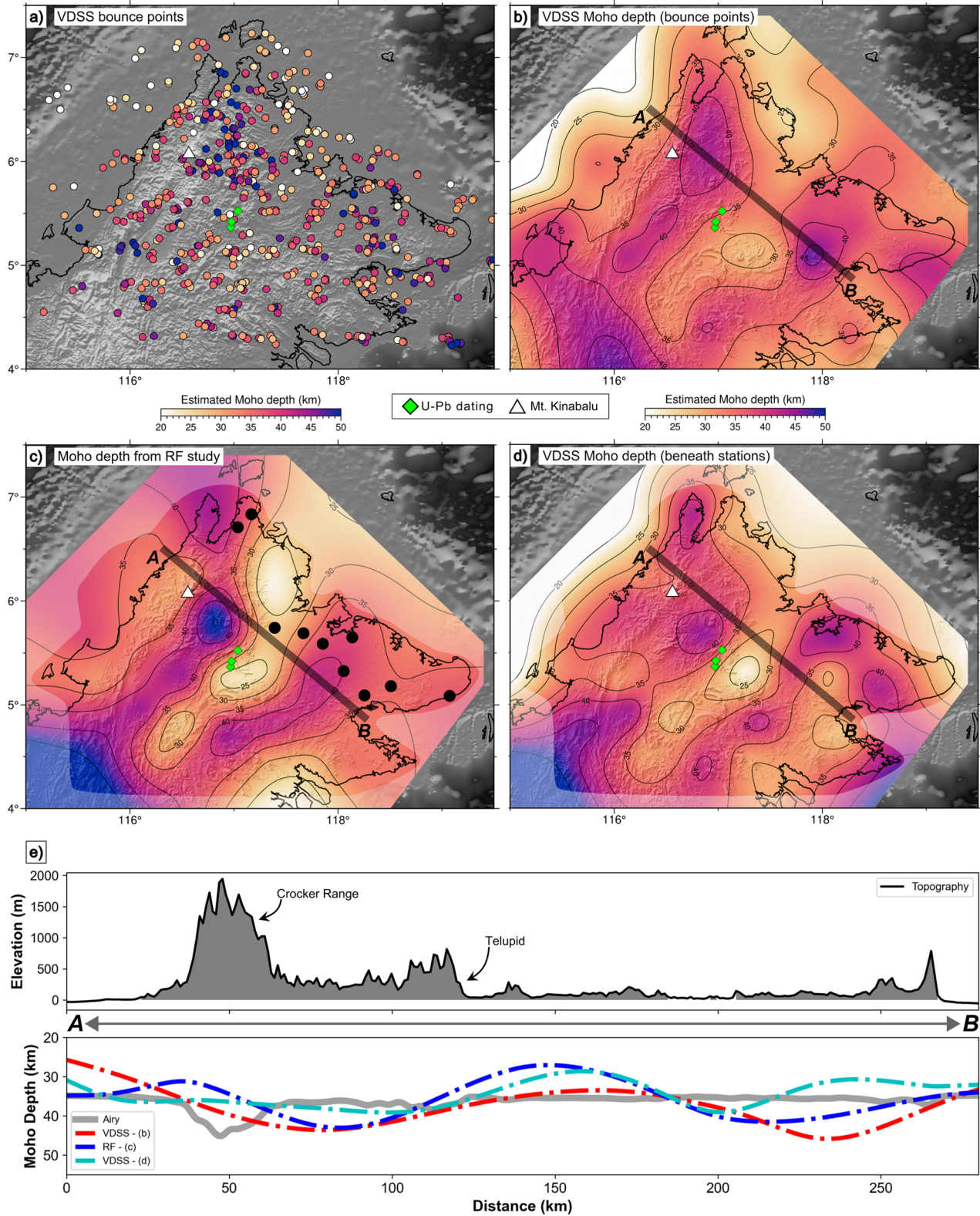


Figure 3.

between the two arrival-time residuals (Δt) is used to adjust the $T_{\text{SsPmp-Ss}}$ travel time, thus mitigating the effect of mantle heterogeneity located between and beneath the virtual source and the receiver. For northern Borneo, we used the S-wave relative arrival-time residuals from Pilia et al. (2022). The average difference between the VDSS traces obtained using method B with and without the incorporation of the calculated Δt is 1.6 ± 0.5 km, which is relatively small and within an acceptable error range. These findings suggest that the influence of mantle heterogeneities in our results would be minimal (see Figure S3 in Supporting Information S1), and are supported by the similarity between Figures 3b and 3d, as noted previously.

The joint RF and surface-wave inversion works well in many parts of northern Borneo but proved challenging in the east due to extensive sedimentary basins and the presence of shallow ophiolite cover. The higher frequency content (e.g., 0.05–2 Hz) used by RFs appears to be more contaminated by short-period noise and reverberations such that primary phase Ps is not easily identifiable (Figure S4 in Supporting Information S1). For VDSS, the SsPmp phase recorded in eastern Sabah is more discernible due to the low-frequency content inherent to the method (0.05–0.5 Hz), which suppresses undesirable signals arising from small-scale intra-crustal structures (Figure S5 in Supporting Information S1).

We choose to show our crustal thickness results assuming that Moho depth estimates are defined at the Pmp reflection points using method A (Figures 3a and 3b) and beneath the stations using method B (Figure 3d). When compared to crustal thicknesses derived from RF analysis (Figure 3c) and inferred from the shear wave velocity structure (Greenfield et al., 2022), all four results appear broadly consistent (e.g., Figure 3e), showing roughly similar Moho depth patterns. As such, we do not particularly favor one VDSS model over the other since they both exhibit the first-order features we interpret. However, VDSS has the advantage of obtaining robust depth estimates in the east, where a clear Moho was absent in the RF results (see Figure 3c and Figure S6 in Supporting Information S1). The robustness of the VDSS results was investigated by constructing Moho maps using the mean SsPmp reflection points as the depth measurement location for different subsets of events (see Figure S7 in Supporting Information S1). We also vary the input crustal velocity model used for the depth-migration of each VDSS trace by adding random noise (Figure S8 in Supporting Information S1). Overall, our analysis suggests that the features that we interpret are well-constrained by the data.

The most abrupt deflection of the Moho inferred by our results appears to coincide with the Crocker Range, where crustal thickness estimates exceed 40 km in places (Figure 3b and 3d). This observation suggests that folding and thrusting due to continent-continent collision between western Sabah and the Dangerous Grounds has produced a thicker crust with a substantial root beneath the mountain belt along the western coast. The Crocker Range is characterized by a Bouguer gravity low (Holt, 1998), indicating that the topography of the mountain belt could be nearly or fully compensated by the crustal root. We further test the state of isostatic compensation by comparing our seismically constrained Moho depths with predictions from an Airy model assuming densities of 1,030, 2,800, and 3,300 kg m⁻³ for water, crust, and mantle, respectively, and using topography data from model SRTM90 (see map in Figure S9 in Supporting Information S1). We also assume a crustal thickness of 35 km prior to continental collision. Figure 3e indicates that the calculated Airy Moho and the observed seismic Moho beneath the Crocker Range are roughly comparable, suggesting that the mountain belt may be isostatically compensated. By assuming the densities and zero-elevation crustal thickness described earlier, the Airy model would imply a shortening of about 22% for an average elevation of the Crocker Range of approximately 1,500 m. An important observation is the landward (SE) lateral offset of ~30 km between the topographic load and the maximum crustal thickness, also observed for example, in the Zagros (Paul et al., 2006), United Arab Emirates-Oman Mountain range (Ali et al., 2020; Pilia, Ali, et al., 2021) and European Alps (Kummerow et al., 2004). It is possible that the topographic load flexed the lithosphere down, and a localized mechanical weakness in the crust may have caused a steepening of the Moho away from the location of the maximum load. Immediately offshore to the west of the Crocker Range on the continental shelf, the crust is significantly thinner, a result largely compatible with Moho

Figure 3. Moho depth maps of northern Borneo. (a) Virtual Deep Seismic Sounding (VDSS) reflection points are plotted as circles and color-coded by Moho depth. (b) Final Moho depth map produced from the interpolation of crustal depths at reflection points (method A), as shown in panel (a). (c) Moho depth map from receiver function study presented in Pilia, Davies, et al. (2021). (d) Moho depth map produced from the interpolation of crustal depths (obtained from stacked VDSS traces) assumed to be below the stations (method B). (e) Elevation and Moho depth cross-section profiles taken from A to B. Green diamonds show the location of ophiolites of Late Miocene age, as inferred by Tsikouras et al. (2021). The white triangle denotes Mt. Kinabalu (4,095 m). Thin black lines in panels (b–d) are depth-to-Moho contours drawn every 5 km. Black-filled circles in panel c represent seismic stations where it is challenging to robustly estimate Moho depth using receiver function. Thick NE-SW black lines in panels (b–d) show the cross-section profiles shown in panel (e). Panels (c and d) include a mask to indicate where the Moho is less well constrained. GMT's "surface" routine, which utilizes splines under tension, was used to achieve a smooth interpolation in panels (b–d) (Wessel et al., 2019).

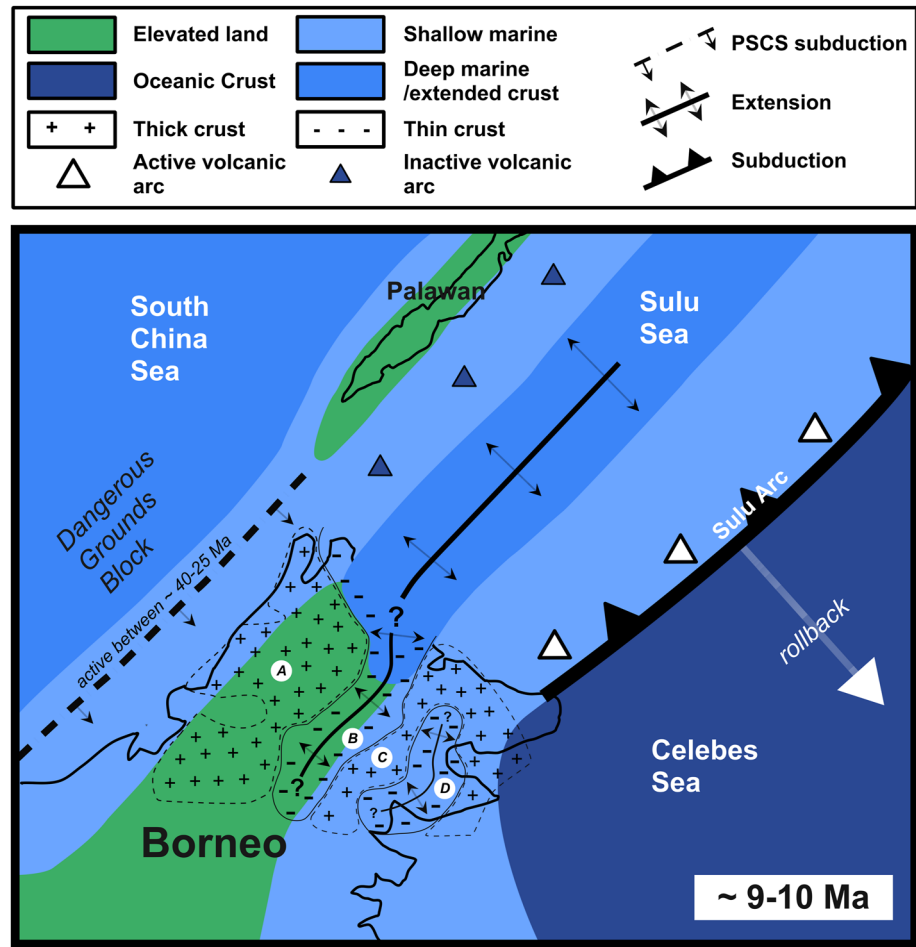


Figure 4. A sketch of the subduction polarity reversal induced tectonic evolution of northern Borneo (adapted from Hall (2013) and Tsikouras et al. (2021)). A and C represent areas of relatively thick crust, while B and D represent areas of relatively thin crust. The triangles represent active (Sulu Arc) and inactive (remnant, submerged) volcanic arcs.

depth inferences made from offshore active seismic methods (Franke et al., 2008). To the southeast, variations in Moho depth do not appear to correlate with the topography, which may be due to a combination of their wavelength and lack of isostatic equilibrium, given the relatively recent cessation of Celebes Sea subduction.

4. Discussion

A significant result that emerges from this study is the area of thin crust in central Sabah (crust B in Figure 4), with a strike similar to the Crocker Range and NW margin of Sabah. The thin crust is wider at the northeast coast and appears to continue offshore into the Sulu Sea. New radiometric data from Tsikouras et al. (2021) indicate that the chemical signature of the Telupid ophiolite represents that of a narrow oceanic basin. The zircons from the ophiolite are Miocene in age (~9.2–9.5 Ma), consistent with the timing of back-arc extension induced by slab roll-back of the Celebes Sea. Intriguingly, the area of thin crust inferred by our results correlates with the mapped exposure of the Telupid ophiolite and the zircon samples analyzed by Tsikouras et al. (2021). We interpret this area of thin crust as evidence of Miocene extension tectonics likely related to the same back-arc extension that formed the Sulu Sea. Brun et al. (2016) suggest that an acceleration in trench retreat in the Aegean changed the region's extension mode from localized to distributed. Northern Borneo might have experienced a similar episode during a period of rapid trench roll-back of the Celebes Sea starting ~16 Ma, as suggested by Hall (2013). During this time, extension in the Sulu Sea may have propagated to the SW, thus forming the areas of thin crust we observe in Sabah.

In the eastern half of Sabah, the Moho depth map reveals an alternating thick and thin crustal pattern (Figure 3b). Despite being narrower than the thick crust labeled A in Figure 4, crust C similarly displays Moho depths of more than 40 km along its strike (see Figure 3d). Further southeast, the thin crust that underlies the Tawau area (crust D in Figure 4) could also have resulted from back-arc extension. This is consistent with extensional tectonics, where strain localization produces thinner crust between thicker and presumably more resistant blocks, somewhat akin to the style of crustal-scale boudinage observed in the Aegean (Jolivet et al., 2004).

The overall pattern of crustal thickness variations determined in this study is consistent with SPR induced by continent-continent collision. In this scenario, intra-oceanic subduction of the PSCS leads to the continent-continent collision of the Dangerous Grounds Block and northern Borneo, which gives rise to the Crocker Range, the root of which is clearly revealed in Figure 3. This is followed by slab break-off, with recent tomographic images from nBOSS data (Pilia et al., 2021a, 2022) showing clear evidence for PSCS slab remnants in the upper mantle and initiation of Celebes Sea subduction. Roll-back of the Celebes Sea slab produces rifting in the back-arc that goes on to form the Sulu Sea in the northeast, but only causes localized extension in northern Borneo (see Figure 3) owing to the presence of continental crust. This entire sequence of events took place over a period of <20 million years, which is comparable to the Laurentian SPR episode discussed by Gasser et al. (2022) and the 2-D SPR numerical simulation of the Solomon back-arc basin by Wang et al. (2022). The continent-continent collision-induced SPR in northern Borneo sets it apart from observations and numerical models of arc-continent and arc-plateau collision (e.g., Almeida et al., 2022; Gasser et al., 2022; Hagke et al., 2016; Stern & Gerya, 2018; Wang et al., 2022) in several ways, including localized back-arc rifting of continental crust and a more substantial mountain range.

5. Conclusions

Based on our new crustal model and other recent geochemical and seismic imaging work, our primary findings are that northern Borneo appears to be a strong candidate for SPR induced by continent-continent collision. Crustal thickness variations are consistent with the sequence of events that typically accompany SPR and the duration of the entire episode (~20 Myr) is in line with findings from other observational and numerical studies. One break with the current understanding of SPR is that substantial portions of continental lithosphere collided, which likely explains the localized extension in the back-arc of the younger subduction system within northern Borneo, compared to the formation of the Sulu Sea further to the northeast. These new findings are highly relevant to those who study Southeast Asian tectonics, SI, and in particular the rapidly evolving field of SPR, where to date observations and numerical modeling have been limited to (arc-or-plateau)-continent collision.

Data Availability Statement

The filtered and sliced waveform data (VDSS traces) for northern Borneo seismic stations can be downloaded from <https://doi.org/10.5281/zenodo.6872172>. Data analysis was carried out using C Shell and Python (3.7). The following Python packages were used: ObsPy (1.2.2, Beyreuther et al., 2010) and Numpy (1.21.3, Harris et al., 2020). Data visualization performed using Generic Mapping Tools (6.0, Wessel et al., 2019) and Matplotlib (3.4.3, Hunter, 2007).

References

- Ali, M. Y., Watts, A. B., Searle, M. P., Keats, B., Pilia, S., & Ambrose, T. (2020). Geophysical imaging of ophiolite structure in the United Arab Emirates. *Nature Communications*, 11(1), 1–10. <https://doi.org/10.1038/s41467-020-16521-0>
- Almeida, J., Riel, N., Rosas, F. M., Duarte, J. C., & Schellart, W. P. (2022). Polarity-reversal subduction zone initiation triggered by buoyant plateau obstruction. *Earth and Planetary Science Letters*, 577, 117195. <https://doi.org/10.1016/j.epsl.2021.117195>
- Beyreuther, M., Barsch, R., Krischer, L., Megies, T., Behr, Y., & Wassermann, J. (2010). ObsPy: A Python toolbox for seismology. *Seismological Research Letters*, 81(3), 530–533. <https://doi.org/10.1785/gssrl.81.3.530>
- Brocher, T. M. (2005). Empirical relations between elastic wavespeeds and density in the Earth's crust. *Bulletin of the Seismological Society of America*, 95(6), 2081–2092. <https://doi.org/10.1785/0120050077>
- Brun, J., Faccenna, C., Gueydan, F., Sokoutis, D., Philippon, M., Kydonakis, K., & Gorini, C. (2016). The two-stage Aegean extension, from localized to distributed, a result of slab rollback acceleration. *Canadian Journal of Earth Sciences*, 53(11), 1142–1157. <https://doi.org/10.1139/cjes-2015-0203>
- Franke, D., Barckhausen, U., Heyde, I., Tingay, M., & Ramli, N. (2008). Seismic images of a collision zone offshore NW Sabah/Borneo. *Marine and Petroleum Geology*, 25(7), 606–624. <https://doi.org/10.1016/j.marpetgeo.2007.11.004>

Acknowledgments

We thank MetMalaysia for allowing access to their restricted data. H.T.L. acknowledges the fieldwork grant awarded by the University of Cambridge's LWA Research Fund and St Edmunds' Cherry Hume Prize. S.P. acknowledges support from the Natural Environmental Research Council (NERC) Grant NE/R013500/1 and the European Union's Horizon 2020 program under Marie Skłodowska-Curie Grant Agreement 790203. We thank NERC's Geophysical Equipment Facility for loan 1038. Seismic data from the nBOSS network will be accessible through the IRIS Data Management Center (<http://www.iris.edu/mda>) from February 2023 (see https://doi.org/10.7914/SN/YC_2018). Waveform data recorded by the nBOSS network were processed and archived by C. A. Bacon. Details on the status of this database may be obtained from N.R.

- Gasser, D., Grenne, T., Corfu, F., Bøe, R., Røhr, T. S., & Slagstad, T. (2022). Concurrent MORB-type and ultrapotassic volcanism in an extensional basin along the Laurentian Iapetus margin: Tectonomagmatic response to Ordovician arc-continent collision and subduction polarity flip. *Bulletin of the Geological Society of America*, *134*(7–8), 1635–1659. <https://doi.org/10.1130/B35970.1>
- Greenfield, T., Gilligan, A., Pilia, S., Cornwell, G. D., Tongkul, F., Widiyantoro, S., & Rawlinson, N. (2022). Post-subduction tectonics of Sabah, northern Borneo, inferred from surface wave tomography. *Geophysical Research Journals: Solid Earth*, *49*(3). <https://doi.org/10.1029/2021GL096117>
- Hagke, C. V., Philippon, M., Avouac, J., & Gurnis, M. (2016). Origin and evolution of subduction polarity reversal from plate kinematics of Southeast Asia. *Geology*, *44*(8), 659–662. <https://doi.org/10.1130/G37821.1>
- Hall, R. (2013). Contraction and extension in northern Borneo driven by subduction rollback. *Journal of Asian Earth Sciences*, *76*, 399–411. <https://doi.org/10.1016/j.jseas.2013.04.01>
- Hall, R., & Breitfeld, H. T. (2017). Nature and demise of the Proto-South China Sea. *Bulletin Geological Society of Malaysia*, *63*, 61–76. <https://doi.org/10.7186/bgsm63201703>
- Hall, R., van Hattum, M. W. A., & Spakman, W. (2008). Impact of India-Asia collision on SE Asia. The record in Borneo. *Tectonophysics*, *451*(1–4), 366–389. <https://doi.org/10.1016/j.tecto.2007.11.058>
- Harris, C. R., Millman, K. J., van der Walt, S. J., Gommers, R., Virtanen, P., Cournapeau, D., et al. (2020). Array programming with NumPy. *Nature*, *585*(7825), 357–362. <https://doi.org/10.1038/s41586-020-2649-2>
- Helffrich, G. (2006). Extended-time multitaper frequency domain cross-correlation receiver-function estimation. *Bulletin of the Seismological Society of America*, *96*(1), 344–347. <https://doi.org/10.1785/0120050098>
- Holt, R. A. (1998). *The gravity field of Sundaland-acquisition, assessment and interpretation, (Doctoral thesis)*. University College London. Retrieved from <https://discovery.ucl.ac.uk/id/eprint/1317811>
- Hunter, J. D. (2007). Matplotlib: A 2D graphics environment. *Computing in Science & Engineering*, *9*(3), 90–95. <https://doi.org/10.1109/MCSE.2007.55>
- Hutchison, C. S., Bergman, S. C., Swauger, D. A., & Graves, J. E. (2000). A Miocene collisional belt in north Borneo. Uplift mechanism and isostatic adjustment quantified by thermochronology. *Journal of the Geological Society*, *157*(4), 783–793. <https://doi.org/10.1144/jgs.157.4.783>
- Jolivet, L., Famin, V., Mehl, C., Parra, T., Aubourg, C., Hebert, R., & Philippot, P. (2004). *Strain localization during crustal-scale boudinage to form extensional metamorphic domes in the Aegean Sea* (Vol. 380, pp. 185–210). Geological Society of London Special Publication. <https://doi.org/10.1130/0-8137-2380-9.185>
- Kennett, B. L. N., Engdahl, E. R., & Buland, R. (1995). Constraints on seismic velocities in the Earth from traveltimes. *Geophysical Journal International*, *122*(1), 108–124. <https://doi.org/10.1111/j.1365-246X.1995.tb03540.x>
- Kummerow, J., Kind, R., Oncken, O., Giese, P., Ryberg, T., Wylegalla, K., & Scherbaum, F. (2004). A natural and controlled source seismic profile through the eastern Alps: TRANSALP. *Earth and Planetary Science Letters*, *225*(1–2), 115–129. <https://doi.org/10.1016/j.epsl.2004.05.040>
- Lai, C. K., Xia, X. P., Hall, R., Meffre, S., Tsikouras, B., Rosana Balangue-Tarriela, M. I., et al. (2021). Cenozoic evolution of the Sulu Sea arc-basin system. An overview. *Tectonics*, *40*(2), 1–26. <https://doi.org/10.1029/2020TC006630>
- Liu, T., Klemperer, S. L., Yu, C., & Ning, J. (2018). Post-critical SsPmp and its applications to Virtual Deep Seismic Sounding (VDSS)-1: Sensitivity to lithospheric 1-D and 2-D structure. *Geophysical Journal International*, *215*(2), 880–894. <https://doi.org/10.1093/GJI/GGY307>
- Liu, T., Klemperer, S. L., Yu, C., & Ning, J. (2020). Post-critical SsPmp and its applications to Virtual Deep Seismic Sounding (VDSS)-3: Back-projection imaging of the crust-mantle boundary in a heterogeneous lithosphere, theory and application. *Geophysical Journal International*, *223*(3), 2166–2187. <https://doi.org/10.1093/gji/ggaa332>
- Matchette-Downes, H., van der Hilst, R. D., Gilligan, A., & Priestley, K. (2019). Seismological constraints on the density, thickness and temperature of the lithospheric mantle in southwestern Tibet. *Earth and Planetary Science Letters*, *524*, 115719. <https://doi.org/10.1016/j.epsl.2019.115719>
- Morley, C. K., & Back, S. (2008). Estimating hinterland exhumation from late orogenic basin volume, NW Borneo. *Journal of the Geological Society*, *165*(1), 353–366. <https://doi.org/10.1144/0016-76492007-067>
- Morley, C. K., King, R., Hillis, R., Tingay, M., & Backe, G. (2011). Deepwater fold and thrust belt classification, tectonics, structure and hydrocarbon prospectivity. *A review: Earth-Science Reviews*, *104*(1–3), 41–91. <https://doi.org/10.1016/j.earscirev.2010.09.010>
- Parker, E. H., Hawman, R. B., Fischer, K. M., & Wagner, L. S. (2016). Estimating crustal thickness using SsPmp in regions covered by low-velocity sediments: Imaging the Moho beneath the southeastern suture of the Appalachian margin experiment (SESAME) array, SE Atlantic coastal plain. *Geophysical Research Letters*, *43*(18), 9627–9635. <https://doi.org/10.1002/2016GL070103>
- Paul, A., Kaviani, A., Hatzfeld, D., Vergne, J., & Mokhtari, M. (2006). Seismological evidence for crustal-scale thrusting in the Zagros mountain belt (Iran). *Geophysical Journal International*, *166*(1), 227–237. <https://doi.org/10.1111/j.1365-246x.2006.02920.x>
- Pilia, S., Ali, M. Y., Searle, M. P., Watts, A. B., Lü, C., & Thompson, D. A. (2021). Crustal structure of the UAE-Oman mountain range and Arabian rifted passive margin: New constraints from active and passive seismic methods. *Journal of Geophysical Research: Solid Earth*, *126*(4). <https://doi.org/10.1029/2020JB021374>
- Pilia, S., Davies, D. R., Hall, R., Bacon, C., Gilligan, A., Greenfield, et al. (2021). Effects of post-subduction processes on continental lithosphere. <https://doi.org/10.21203/rs.3.rs-861968/v1>
- Pilia, S., Rawlinson, N., Gilligan, A., & Tongkul, F. (2019). Deciphering the fate of plunging tectonic plates in Borneo. *Eos, Transactions - American Geophysical Union*, *100*, 18–23. <https://doi.org/10.1029/2019EO123475>
- Pilia, S., Rawlinson, N., Hall, R., Cornwell, D., Gilligan, A., & Tongkul, F. (2022). Seismic signature of subduction termination from teleseismic P- and S-wave arrival-time tomography: The case of northern Borneo. *Earth and Space Science Open Archive*. <https://doi.org/10.1002/essoar.10511094.1>
- Stern, R. J., & Gerya, T. (2018). Subduction initiation in nature and models: A review. *Tectonophysics*, *746*, 173–198. <https://doi.org/10.1016/j.tecto.2017.10.014>
- Thompson, D. A., Rawlinson, N., & Tkalčić, H. (2019). Testing the limits of virtual deep seismic sounding via new crustal thickness estimates of the Australian continent. *Geophysical Journal International*, *218*(2), 797–800. <https://doi.org/10.1093/gji/ggz191>
- Tongkul, F. (1994). The geology of Northern Sabah, Malaysia: Its relationship to the opening of the South China Sea Basin. *Tectonophysics*, *235*(1–2), 131–147. [https://doi.org/10.1016/0040-1951\(94\)90021-3](https://doi.org/10.1016/0040-1951(94)90021-3)
- Tongkul, F. (1997). Polyphase deformation in the Telupid area, Sabah, Malaysia. *Journal of Asian Earth Sciences*, *15*(2–3), 175–183. [https://doi.org/10.1016/S0743-9547\(97\)00006-8](https://doi.org/10.1016/S0743-9547(97)00006-8)
- Tongkul, F. (2017). Active tectonics in Sabah – Seismicity and active faults. *Bulletin Geological Society of Malaysia*, *64*(1), 27–36. <https://doi.org/10.7186/bgsm64201703>

- Tseng, T. L., Chen, W. P., & Nowack, R. L. (2009). Northward thinning of Tibetan crust revealed by virtual seismic profiles. *Geophysical Research Letters*, *36*(24), 1–5. <https://doi.org/10.1029/2009GL040457>
- Tsikouras, B., La, C. K., Ifandi, E., Norazme, N. A., Teo, C. H., & Xia, X. P. (2021). New zircon radiometric U-Pb Ages and Lu-Hf isotopic data from the ultramafic-mafic sequences of Ranau and Telupid (Sabah, East Malaysia): Time to reconsider the geological evolution of Southeast Asia? *Geology*, *49*(7), 789–793. <https://doi.org/10.1130/G48126.1>
- Wang, L., Dai, L., Gong, W., Li, S., Jiang, X., Foulger, G., et al. (2022). Subduction initiation at the Solomon back-arc basin: Contributions from both island arc rheological strength and oceanic plateau collision. *Geophysical Research Letters*, *49*(3), 1–11. <https://doi.org/10.1029/2021GL097666>
- Wessel, P., Luis, J., Uieda, L., Scharroo, R., Wobbe, F., Smith, W., & Tian, D. (2019). The generic mapping tools version 6. *Geochemistry, Geophysics, Geosystems*, *20*(11), 5556–5564. <https://doi.org/10.1029/2019GC008515>
- Yang, G. (2022). Subduction initiation triggered by collision: A review based on examples and models. *Earth-Science Reviews*, *232*, 104129. <https://doi.org/10.1016/j.earscirev.2022.10>
- Yu, C., Chen, W., & Hilst, R. D. (2016). Constraints on residual topography and crustal properties in the Western United States from virtual deep seismic sounding. *Journal of Geophysical Research: Solid Earth*, *121*(8), 5917–5930. <https://doi.org/10.1002/2016JB013046>
- Yu, C. Q., Chen, W. P., & van der Hilst, R. D. (2013). Removing source-side scattering for Virtual Deep Seismic Sounding (VDSS). *Geophysical Journal International*, *195*(3), 1932–1941. <https://doi.org/10.1093/gji/ggt359>